μFLU08–118

AN INTERFACE CAPTURING METHOD FOR TWO–PHASE FLOW WITH MOVING CONTACT LINES

Sara Zahedi[1]
Royal Institute of Technology, CSC/NA, 100 44 Stockholm, Sweden
sara7@csc.kth.se

Gunilla Kreiss, Katarina Gustavsson
Uppsala University, 751 05 Uppsala, Sweden,
Royal Institute of Technology, CSC/NA, 100 44 Stockholm, Sweden
gunillak@it.uu.se, katarina@csc.kth.se

KEY WORDS

contact line dynamics, contact angle, level set method, two phase flow, conservative method

ABSTRACT

This paper presents a conservative numerical method capable of capturing contact line movement for the simulation of capillary dominated flow of two immiscible, incompressible fluids. The interface between the two fluids is represented implicitly by the 0.5–level set of a function varying smoothly from zero to one. The flow of each phase is governed by the incompressible Navier–Stokes equations with no–slip boundary condition at solid walls. The key idea is to drive the contact line movement by prescribing the normal vector at the boundary to be the static normal vector corresponding to the equilibrium contact angle. Our model is formulated as a system of partial differential equations and takes into account differences in density and viscosity, gravity, and surface tension effects. We discretize using the finite element method which allows for use of the weak form of the equations. The surface tension forces are included as line integrals along the interfaces. We eliminate the second order derivatives in these forces, coming from the curvature term, by applying partial integration of the Laplace–Beltrami operator. Numerical experiments of capillary dominated flows in two space dimensions are presented and include tests of convergence rates and comparison with other numerical methods. Our numerical scheme show good accuracy and our results compare well with available theory.

1. INTRODUCTION

Accurate modeling and simulations of contact line movement is of crucial interest in simulations of 1) two–phase flow in microfluidic devices, such as pumps, valves, separators etc, 2) inkjet printing, spray coating, and spray cooling, and 3) two–(or multi–)phase flow in pore structures occurring for example when oil is recovered by water injection and in liquid phase sintering. In all these cases simulations can contribute to a better understanding of the process considered.

Contact line dynamics is the movement of the intersection line between the interface of two immiscible fluids and a solid boundary. An example of such a phenomenon is when a liquid drop is spreading over a solid surface. As the drop spreads, the contact line will move until it reaches an equilibrium state determined by the surface energies of the interfaces involved. The angle between the contact line at equilibrium and the boundary is often referred to as the equilibrium or static contact angle (hereinafter, *the static contact angle*). For a more detailed discussion of this kind of phenomena see [1].

[1] Corresponding author

The immiscible and incompressible flow is described by the incompressible Navier–Stokes equations with the surface tension forces and gravity forces added as source terms. Some representation of the interface separating the two fluids is required, for example a level set function or markers, and an evolution equation for the advection of the interface. At all interior points, the physically correct model is that the interface is advected by the fluid velocity. At contact lines, however, the standard boundary condition for the velocity is no–slip, which means that the contact line cannot move. This is unphysical in many cases, which is reflected by the shear stress becoming singular. Over the years, various techniques to overcome this difficulty have been introduced. One direction is to introduce a so called slip length, which permits the contact line to move, see for instance [2] and references therein. The difficulty with this approach is to provide an appropriate value for the slip coefficient. The existence of fluid–wall slipping has been observed in molecular dynamics simulations, see [3] and references therein. Another approach was suggested by Jacqmin [4] who used a coupled Cahn–Hilliard/ Navier–Stokes formulation consisting of the Navier–Stokes equations coupled to a system of two parabolic equations for the chemical potential and the concentration of one of the fluids. In this model, the interface is modeled as a layer with a continuous transition from one fluid to the other, and the contact line as a small region; the part of the interface layer close to the solid boundary. The contact line moves by diffusive processes on a fast time scale in the small region at the boundary so that the contact angle is adjusted to the static value. The result is a region close to the boundary with high curvature of the interface, and consequently a strong surface tension force. The fact that the interface can move by diffusive processes eliminates the need for modeling fluid slip. A drawback with the model suggested by Jacqmin is that the interface must be highly resolved to achieve accuracy. In [5] this formulation was used to investigate basic wetting phenomena.

A new level set method for two phase flow with good mass conservation of each fluid was introduced in [6] and [7]. In this method the interface is represented implicitly by the 0.5–level set of a regularized Heaviside function ϕ. By construction, the method conserves $\int \phi$. We have extended this method to be able to capture contact–line movement while retaining the conservative property [8, 9]. The new model mimics the Cahn–Hilliard/Navier–Stokes behavior of the interface at solid walls by using diffusion to move the contact point. Compared to the standard Cahn–Hilliard/Navier–Stokes formulation we believe the new model reduces the needed computational effort, since a relatively coarse grid is sufficient to capture the dynamics, at least away from contact points. In this work we use an improved representation of the surface tension, based on partial integration of the Laplace–Beltrami operator, see [10, 11] and references therein. In this way we avoid computation of the curvature. We also present new computations, where viscosity and density of the fluids differ. All our computations are in two space dimensions, but there is no principal difficulty to extend the method to three space dimensions.

The paper is organized as follows. In section 2 we present the governing equations of the model and give a description of our interface representation and the numerical method. The treatment of the surface tension force based on partial integration of the Laplace–Beltrami operator is explained. In section 3, we use the model in three different applications; the spreading of a droplet on a flat plate, the rising of a droplet and a channel flow. Section 4 contains a summary and a discussion of possible improvements of the model.

2. MATHEMATICAL MODEL AND NUMERICAL METHOD

The fundamental model of two–phase flow with contact line dynamics consists of the incompressible Navier–Stokes equations coupled with evolution of the interface. Evolution of the interface is, in this work, achieved by use of the advection equation together with a reinitialization step. In this section we will present this model and how it is treated numerically.

2.1 The Incompressible Navier–Stokes Equations

Assume a given domain Ω is occupied by two immiscible fluids separated by an interface Γ. The equations describing this immiscible flow are the incompressible Navier–Stokes equations with the contribution of the surface tension forces and the gravity forces added as source terms:

$$Re\left((\rho\mathbf{u})_t + \nabla\cdot(\rho\mathbf{u}\mathbf{u})\right) = -Re\nabla p + \nabla\cdot\left(\mu\left(\nabla\mathbf{u} + (\nabla\mathbf{u})^T\right)\right) + \frac{Re}{Fr^2}\rho\mathbf{e}_g + \frac{1}{Ca}\kappa\mathbf{n}\delta_\Gamma, \tag{1}$$

$$\nabla \cdot \mathbf{u} = 0.$$

Here $\mathbf{u}$, p, ρ and μ denote velocity, pressure, density, and viscosity, respectively. In general ρ and μ are discontinuous across the interface separating the two fluids. The curvature and normal of the interface Γ are denoted by κ and $\mathbf{n}$, and δ_Γ is a Dirac delta function with support on Γ. Its action on any smooth test function v is given by

$$\int_\Omega \delta_\Gamma v d\Omega = \int_\Gamma v d\Gamma. \tag{2}$$

The direction of gravitation is denoted by $\mathbf{e}_g$. The equations are formulated on a non–dimensional form where the dimensionless Reynolds, Capillary and Froude numbers are given by

$$Re = \frac{\rho_{\text{ref}} u_{\text{ref}} l_{\text{ref}}}{\mu_{\text{ref}}},\ Ca = \frac{\mu_{\text{ref}} u_{\text{ref}}}{\sigma},\ \text{and}\ Fr = \frac{u_{\text{ref}}}{\sqrt{l_{\text{ref}} g}}. \tag{3}$$

Here ρ_{ref}, μ_{ref}, l_{ref}, and u_{ref} are constant reference density, viscosity, length and velocity. The coefficient σ is the surface tension coefficient and g is the gravitational constant. The Reynolds number is the ratio between inertial and viscous forces. The Capillary number gives the ratio between the viscous and surface tension forces and the Froude number gives a measure of the ratio between inertial and gravitational forces.

In order to complete the formulation, a representation of the interface and a model for its motion are needed. This will be addressed in the next subsection.

2.2 An Improved Level set Representation of the Interface

Level set representations of the interface in two phase flow have been used in many flow situations, see for instance [12] or [13]. The basic idea is that if a level set of a function ϕ_0 defines the interface at $t = 0$, the same level set of the solution to

$$\phi_t + \nabla \cdot (\phi \mathbf{u}) = 0,\ \phi(\cdot, 0) = \phi_0, \tag{4}$$

defines the interface at later times.

The method proposed in this paper is an extension of the conservative level set method, introduced in [6]. Instead of the signed distance function [12, 13] usually used to define the interface, this method uses a regularized indicator function ϕ that takes the values 0 and 1 in the two fluids, respectively. The 0.5–level defines the interface. In this way, good conservation properties can be achieved simply by using a conservative discretization. The shape of the regularized step function is controlled in a reinitialization step. This step is modeled by a partial differential equation where a non–linear term, resembling a compressive limiter (see [14]), is balanced by diffusion in the normal direction. In the following we introduce a new reinitialization that can be used to capture contact line dynamics. This is a generalization of the reinitialization procedures used in [6] and [7].

The new model mimics the Cahn–Hilliard/Navier–Stokes model in the following way. Contact points are modeled as regions and diffusion is used to move the contact point so that the angle between the interface, defined by the 0.5–level set of ϕ, and the boundary always equals the static contact angle α_s. The static contact angle corresponds to a normal to the interface $\mathbf{n}_{\alpha_s}$. Since the gradient of the level set function is related to the normal of the interface by $\mathbf{n} = \nabla\phi/|\nabla\phi|$, the condition on the angle can be formulated as a condition on the gradient. We cannot, however, directly prescribe the gradient of the level set function at the boundary without creating a flux of ϕ over the boundary that would destroy the conservative properties of the model.

Our idea is to instead use a regularized normal vector field satisfying

$$\mathbf{n} - \nabla \cdot (\gamma^2 \nabla \mathbf{n}) = \frac{\nabla\phi}{|\nabla\phi|}, \tag{5}$$

with Dirichlet boundary conditions, $\mathbf{n} = \mathbf{n}_{\alpha_s}$ along solid walls. The regularization parameter γ should preferably be chosen $\gamma \ll L$, where L is the length of typical features in the problem at hand. The regularized normal vector will then be close to the gradient of the unperturbed ϕ, except along the boundary, where a boundary

layer with thickness proportional to γ will form. The modified vector field is then used in the reinitialization in the following fashion

$$\phi_{\hat{t}} + \nabla \cdot (\phi(1-\phi)\mathbf{n}) - \nabla \cdot (\varepsilon_n(\nabla\phi \cdot \mathbf{n})\mathbf{n}) - \nabla \cdot (\varepsilon_\tau(\nabla\phi \cdot \mathbf{t})\mathbf{t}) = 0 \tag{6}$$

where $\mathbf{n}$ is the normalized and regularized gradient of ϕ, satisfying (5), and $\mathbf{t}$ is the tangent, orthogonal to $\mathbf{n}$, ε_n is a viscosity parameter in the normal direction and ε_τ is a viscosity parameter in the tangential direction. The second term in (6) represents compression in the normal direction, while the third models diffusion in the normal direction and the last term models diffusion in the tangential direction. In the original work on the conservative level set method [6] the standard isotropic diffusion was used. This corresponds to choosing $\varepsilon_\tau = \varepsilon_n = \varepsilon$ in equation (6). In the subsequent work, presented in [7], $\varepsilon_\tau = 0$. The idea was to avoid unnecessary movement of the 0.5–level set in the tangential direction. However, the tangential diffusion is essential for the contact angle to achieve the desired static value. An alternative is to include diffusion in the advection equation (4).

If our modeling is successful, the solution ϕ will exhibit a boundary layer of thickness proportional to the regularization parameter γ. The angle of the interface (the 0.5–level set of ϕ) to the boundary changes from the static contact angle α_s to the apparent contact angle α_a. The apparent contact angle is the angle formed between the boundary and the interface away from the contact point region. Thus, close to the boundary the curvature will be large. It is important that γ is chosen so that the curvature in this region is numerically resolved. The contact point will move with the same speed as the tangential fluid velocity just outside the contact point region. When the two fluids have the same viscosity it can be shown that for small γ the speed is independent of γ, see [9].

2.3 Numerical Treatment

We solve the Navier–Stokes equations using a projection method with an added pressure stabilization term [7]. This method was introduced by Guermond and Quartapelle [15]. The surface tension effect is treated as a force, $\mathbf{f} = \sigma\kappa\mathbf{n}\delta_\Gamma$ added to the Navier–Stokes equations. Since we consider applications where the capillary effects dominate the accuracy of the surface tension force is essential. In general, the accuracy of the curvature estimation and the implementation of the surface tension force are crucial in order to avoid large unphysical oscillations of the velocity close to the interface, so–called spurious velocities. Using the finite element framework enables us to write the equations in weak form. The weak formulation of the equations does not include δ_Γ and therefore no explicit discretization of the delta function is required. By using the Laplace–Beltrami characterization of the curvature we do not need to calculate the curvature.

Define the tangential derivative of a function g along Γ by $\nabla_\Gamma g = P\nabla g$ where P is the orthogonal projection:

$$P = I - \mathbf{n}\mathbf{n}^T. \tag{7}$$

Replace the term $\kappa\mathbf{n}$ by the Laplace–Beltrami operator

$$\nabla_\Gamma \cdot (\nabla_\Gamma id_\Gamma) = \kappa\mathbf{n}, \tag{8}$$

where id_Γ is the identity on Γ and the normal vector $\mathbf{n}$ is calculated as

$$\mathbf{n} = \frac{\nabla\phi}{|\nabla\phi|}. \tag{9}$$

If $\mathbf{v}$ is a smooth vector valued function on Ω we can integrate by parts to get

$$\begin{aligned} f_\Gamma(\mathbf{v}) &= \frac{1}{Ca}\int_\Omega \kappa\mathbf{n}\cdot\mathbf{v}\delta_\Gamma d\Omega = \frac{1}{Ca}\int_\Gamma \kappa\mathbf{n}\cdot\mathbf{v}d\Gamma = \\ &= \frac{1}{Ca}\int_\Gamma \nabla_\Gamma\cdot(\nabla_\Gamma id_\Gamma)\cdot\mathbf{v}d\Gamma = -\frac{1}{Ca}\int_\Gamma \nabla_\Gamma id_\Gamma\cdot\nabla_\Gamma\mathbf{v}d\Gamma \end{aligned} \tag{10}$$

In our model the boundary conditions for the velocity is no–slip. Hence our test function $\mathbf{v}$ is zero at the contact points and we don't have any boundary terms in the above identity. This technique of reducing the order of differentiation associated with the curvature term has also successfully been applied in the finite element context in [10, 11] and references therein.

At contact points diffusion of ϕ tangential to the interface is essential. In the third application, "Capillary Dominated Channel Flow", we choose to add the diffusion in the reinitialization equation (6) by letting $\varepsilon_\tau = \varepsilon_n$. In the first and the second application, "Droplet on a Flat Plate" and "Rising Droplet", we let $\varepsilon_\tau = 0$ but we add an isotropic diffusion term equal to $5h^2 = 0.0011$ in the advection equation (4). In each time step the reinitialization equation (6) is solved to steady state. As in [7] we use a second order semi–implicit discretization in time with $\Delta\hat{t} = \Delta t$. Typically two steps of reinitialization is performed at each time step.

The numerical simulations were carried out using FemLego (Amberg et al. [16]), a symbolic tool to solve partial differential equations with the finite element method. All equations were discretized in space using piecewise linear functions and the linear systems were solved using conjugate gradient methods.

3. APPLICATIONS

In this section we discuss the numerical treatment and results for three applications in which capillary effects dominate: a droplet on a flat plate, rising droplet and channel flow. All applications involve two immiscible fluids and moving contact lines. The proposed model is used to simulate the contact line dynamics. The results in the application "Droplet on a Flat Plate" is compared with theory and other computations. The two other applications indicate that we can also handle density and viscosity differences.

3.1 Application 1: Droplet on a Flat Plate

We consider here a two–dimensional droplet with diameter l_{ref}, density ρ_{ref}, and viscosity μ_{ref}, lying on a solid surface surrounded by another liquid with the same density and viscosity. The static contact angle is $\alpha_s = 25°$. Capillary effects dominate and gravity is neglected. We will simulate how this droplet wets the surface. This wetting phenomenon was previously studied using a phase field method by Villanueva and Amberg [5]. We will compare our results with data from the phase field simulation and Cox's theory [17].

3.1.1 Computations

The computational domain is in non–dimensional coordinates $\{(x, y) : -2 \leq x \leq 2,\ 0 \leq y \leq 2\}$ and the initial drop is symmetric around $x = 0$ and has non–dimensional radius $r = 0.5$. At initial time the drop is in contact with the solid wall at an angle of $156°$. The Reynolds number $Re = \frac{\rho_{\text{ref}} u_{\text{ref}} l_{\text{ref}}}{\mu_{\text{ref}}} = 1$ and the Capillary number $Ca = \frac{2\sqrt{2}\mu_{\text{ref}} u_{\text{ref}}}{3\sigma} = 1$. The simulation of the wetting is performed using a mesh consisting of regular triangles with 270×135 nodes and a time step $\Delta t = 0.0011$. The liquid–liquid interface (the 0.5–level set of ϕ) is advected by solving the advection equation (4) with a diffusion term equal to $5h^2 = 0.0011$ where $h = \Delta x = \Delta y$ and typically two steps of reinitialization. In the reinitialization described in equation (6) the viscosity parameter in the normal direction is set to $\varepsilon_n = 4.5h = 0.0667$ and the viscosity parameter in the tangential direction is set to $\varepsilon_\tau = 0$. The boundary condition for the velocity is no–slip. For the regularized normal vector field, equation (5) the boundary condition is

$$\mathbf{n}|_{y=0} = (-\text{sign}(x)0.4226, -0.9063)$$

so that the contact angle at the wall is equal to the static contact angle $25°$. At the other boundaries we use homogeneous Neumann conditions. The regularization parameter in equation (5) $\gamma = 0.1667$. We want to choose γ so that the normal vector varies smoothly from the prescribed equilibrium value at the boundary to the actual value. Thus on one hand, a large γ is needed when the dynamic contact angle is large compared to the static contact angle. The static contact angle determines the value of the normal vector at the boundary. On the other hand, if γ is too large, we get too large wetting speed, especially in the initial steps. This was studied in [9]. When γ is decreased, the grid has to be refined. We believe that compared to [9] we should be able to use a smaller γ since we don't need to calculate the curvature. This has however not yet been tested.

In Fig. 1 the wetting on the solid wall is illustrated for six different snapshots. The liquid–liquid interface immediately forms a foot due to the boundary condition for the normal at the wall described above. The strong curvature in the foot region causes the contact line to move and the drop starts to wet the surface. The contact–line movement is fast in the initial steps but slows down as the drop approaches equilibrium. At $t \approx 300$ equilibrium is reached.

We measure the dynamic contact angle that the liquid–liquid interface makes with the solid surface at the inflexion point of the foot as illustrated in Fig. 2(a). The wetting speed is given by dividing the difference in position of the intersection point (see Fig. 2(a)) at two successive times by the time difference. The dynamic contact angle initially decreases rapidly with time but the decrease slows down as the angle approaches the equilibrium value. In Fig. 2 the dependence of the dynamic contact angle on the Capillary number $Ca^* = \frac{2\sqrt{2}\mu_{\text{ref}}u}{3\sigma} = \frac{u}{u_{\text{ref}}}$, which in this case is equal to the wetting speed, is shown. The results are compared with a phase field simulation[5] and Cox's theory[17]. Our simulation shows qualitative agreement with them all. The velocity for each given angle is, in our simulation, somewhat larger than the predictions provided by Cox's theory with the viscosity ratio $\lambda = 1$ and $\delta = 10^{-4}$. See [9] for the choice of δ.

To investigate convergence we have performed computations for three different meshes with $h_1 = 0.0222$, $h_2 = \frac{2}{3}h_1$ and $h_3 = \frac{4}{9}h_1$. All parameters are fixed, the initial contact angle is now 90° and $\gamma = 0.1$. The error is measured as the sum of absolute differences in the y–coordinates for the interface for 100 x–coordinates divided by the number of points. The order of convergence is shown in Fig. 3 both when applying integration by parts of the Laplace–Beltrami operator on the interface and calculating the curvature and then the line integral.

3.2 Application 2: Rising Droplet

We now consider a two–dimensional droplet with density ρ_D and viscosity μ_D lying on a solid surface at an angle of 90° surrounded by a heavier fluid with density $\rho_L = 10\rho_D$ and viscosity $\mu_L = \mu_D$. We make a simulation of the droplet rising.

3.2.1 Computations

The computational domain is in non–dimensional coordinates $\{(x, y) : -1.5 \leq x \leq 1.5,\ 0 \leq y \leq 3\}$. The initial drop is symmetric around $x = 0$ with non–dimensional radius $r = 0.5$. The Reynolds number and the Capillary number are as in the first application "Droplet on a Flat Plate" set to 1 but the gravity cannot be neglected and the Froude number $Fr = \frac{u_{\text{ref}}}{\sqrt{l_{\text{ref}}g}} = 0.7$. The simulation is performed using a mesh consisting of regular triangles with 180×180 nodes and a time step $\Delta t = 0.0011$. The regularization parameter in equation (5) $\gamma = 0.1$. All other parameters are as in the first application "Droplet on a Flat Plate". In Fig. 4 the interface and the velocities at the interface are plotted at a sequence of different times. The drop wants to wet the solid surface but the surrounding fluid is heavier so it starts to rise. At $t \approx 9$ the droplet breaks into two parts, where one part continues to rise and one part remains attached to the lower wall.

3.3 Application 3: Capillary Dominated Channel Flow

Consider two fluids in a two dimensional channel of non–dimensional width 1 and length 1.5, initially separated by an interface, normal to the channel, without curvature. Thus, the initial apparent contact angle is $\alpha_a = 90^\circ$. We assume that the static contact angle α_s is less than 90°, which corresponds to the left fluid wetting the channel walls. Clearly the initial condition is not a steady state solution. In the absence of an outer pressure gradient or a prescribed flux, the only driving force are the capillary effect at the channel walls, which will move the interface to the right. If the densities and viscosities of the two fluids are of similar size we expect that after an initial, transient process, the interface will move at a constant, or in the case of differing fluid properties, slowly varying speed U. We expect the interface to consist of an interior part with curvature $\kappa_a = 2\cos(\alpha_a)$, and two small sections close to the walls with curvature $\kappa \propto \frac{f(\alpha_a - \alpha_s)}{\gamma}$, where f is some smooth function.

We have performed two sets of computations to investigate the qualitative behavior of our model. In the computations in this section the Capillary number and the Reynolds number are set to unity, and both fluids have the same density. At the channel walls we prescribe zero velocity, i.e. no slip, and the flux of the level set function is set to zero. The normal vector is set so that the contact angle at the wall equals the static contact angle. At the inlet and outlet we use vanishing tangential velocity, vanishing normal derivative of the normal velocity, and Dirichlet conditions for the level set function and the pressure. Throughout this section we use $\varepsilon_\tau = \varepsilon_n = 0.025$, $\gamma = 0.05$, $\Delta x = 0.01$ and $\Delta\hat{t} = \Delta t = 0.04$.

In the first set of computations we investigate the effect of the static contact angle on the interface speed. In these computations the fluids have the same viscosity. In Fig. 5 we show the interface together with local velocity vectors during the initial, transient phase. A region of large curvature of the interface develops near

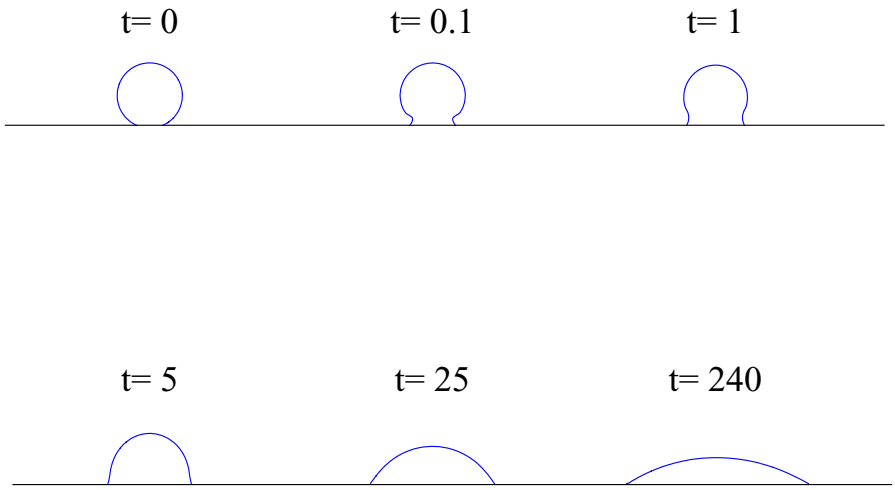

Figure 1: Wetting of a liquid drop on a solid surface. The interface separating the two fluids at times $t = 0, 0.1, 1, 5, 25, 240$ with $Re = 1$, $Ca = 1$. The contact angles at the different times are $\alpha \approx 156, 149, 117, 82, 54, 29$. The regularization parameter $\gamma = 0.1667$.

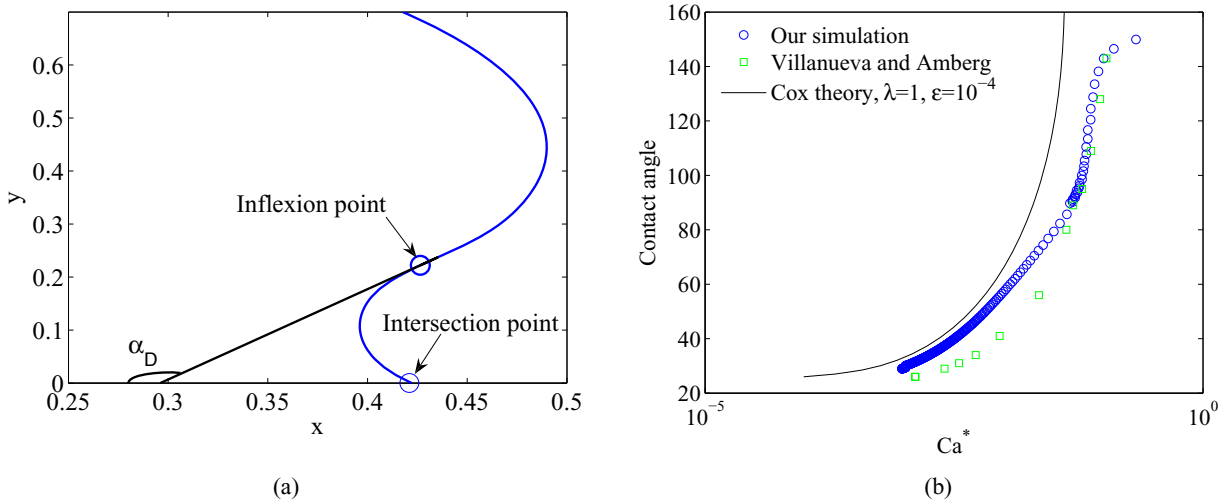

Figure 2: (a): The dynamic contact angle is measured by considering the tangent at the inflexion point. The wetting speed is given from the position of the intersection point at different times. (b) : The dynamic contact angle versus the capillary number. Initial angle is $156°$.

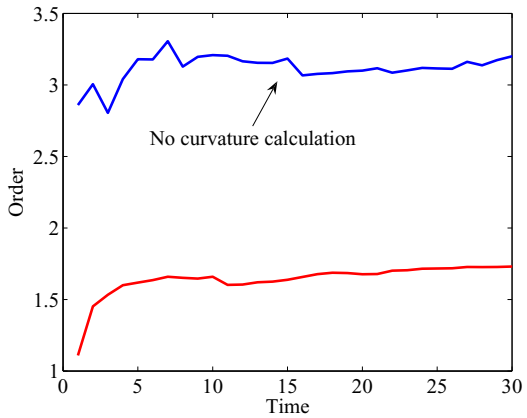

Figure 3: The order of convergence both when applying integration by parts of the Laplace–Beltrami operator on the interface and calculating the curvature and then the line integral. All parameters are fixed, the initial contact angle is $90°$ and $\gamma = 0.1$.

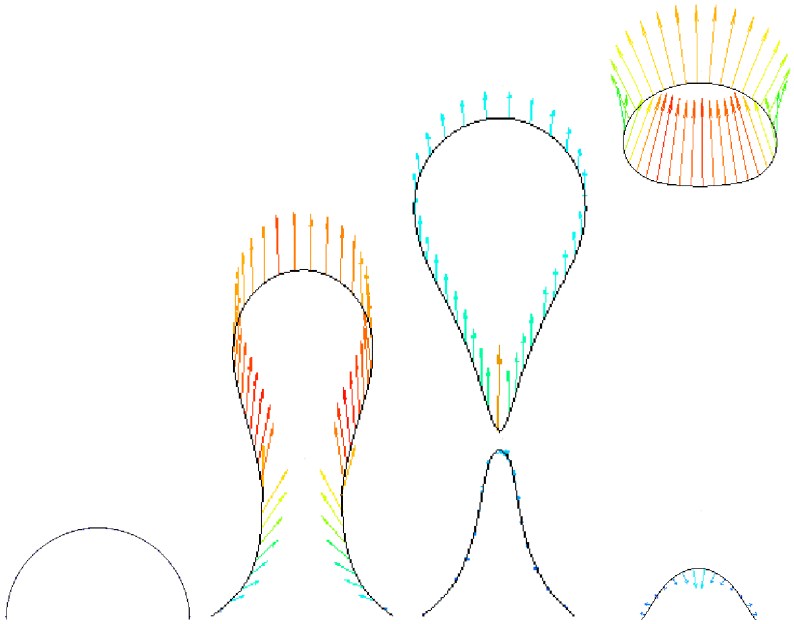

(a) $t = 0$ (b) $t = 7$ (c) $t = 9$ (d) $t = 13$

Figure 4: Rising drop. The location of the interface separating the two fluids at times $t = 0, 7, 9, 13$ with Re=1, Ca=1, Fr=0.7, and $\frac{\rho_L}{\rho_D} = 10$. The arrows show velocities at the interface.

the solid walls. There, the surface tension is strong, resulting in local, large velocities. After $t = 3$ the transient development of the interface is complete, but the curvature and velocities are still large near the wall. Away from the interface the velocity field is close to the standard pipe flow parabola. In Fig. 6 we see the time history of the interface for two different static angles. In both cases an interface shape develops within the first time units, and then propagates with constant speed. As expected, the speed is greater when the static angle is smaller. In the second set of computations we investigate the effect of a difference in fluid viscosity on the interface movement. We let the fluid to the left be more viscous than the fluid to the right. As the interface moves to the right an increasing part of the channel is filled with the more viscous fluid. Thus we expect the interface speed to slow down. In Fig. 7 we see the time history of the interface at an early stage and at a later stage for two different viscosity ratios. It is clear that increasing the difference in viscosity increases the slowing down effect, as expected.

4. CONCLUSIONS

We have developed and presented a conservative level set model for two–phase flow, which can capture contact line dynamics using no–slip boundary conditions for the velocity. In this model, the contact angle at equilibrium is used to induce a movement by diffusion of the contact point. Since the model is formulated in terms of partial differential equations on conservative form, conservation properties are retained by using standard conservative numerical methods.

In our model we have a diffusion parameter and a regularization parameter related to the size of the contact point region. An investigation of where the needed diffusion is best to add, in the advection equation or in the reinitialization, as well as the magnitude of the diffusion term needs to be done. By writing the equations in weak form and using the Laplace–Beltrami operator we have been able to avoid calculation of the curvature. We believe this will enable us to choose a smaller regularization parameter but this remains to be studied. As a further improvement of this model we suggest that the model parameters as well as the new boundary condition should be adaptive and act only locally in small regions close to contact points. Also, adaptive refinement of the mesh in regions with large curvature would be beneficial in order to be able to use smaller values of the parameters. This is especially important for the regularization parameter γ.

Numerical computations for three different applications demonstrate that qualitative features of contact line dynamics are captured. The results from the calculation of the droplet wetting the wall has shown good

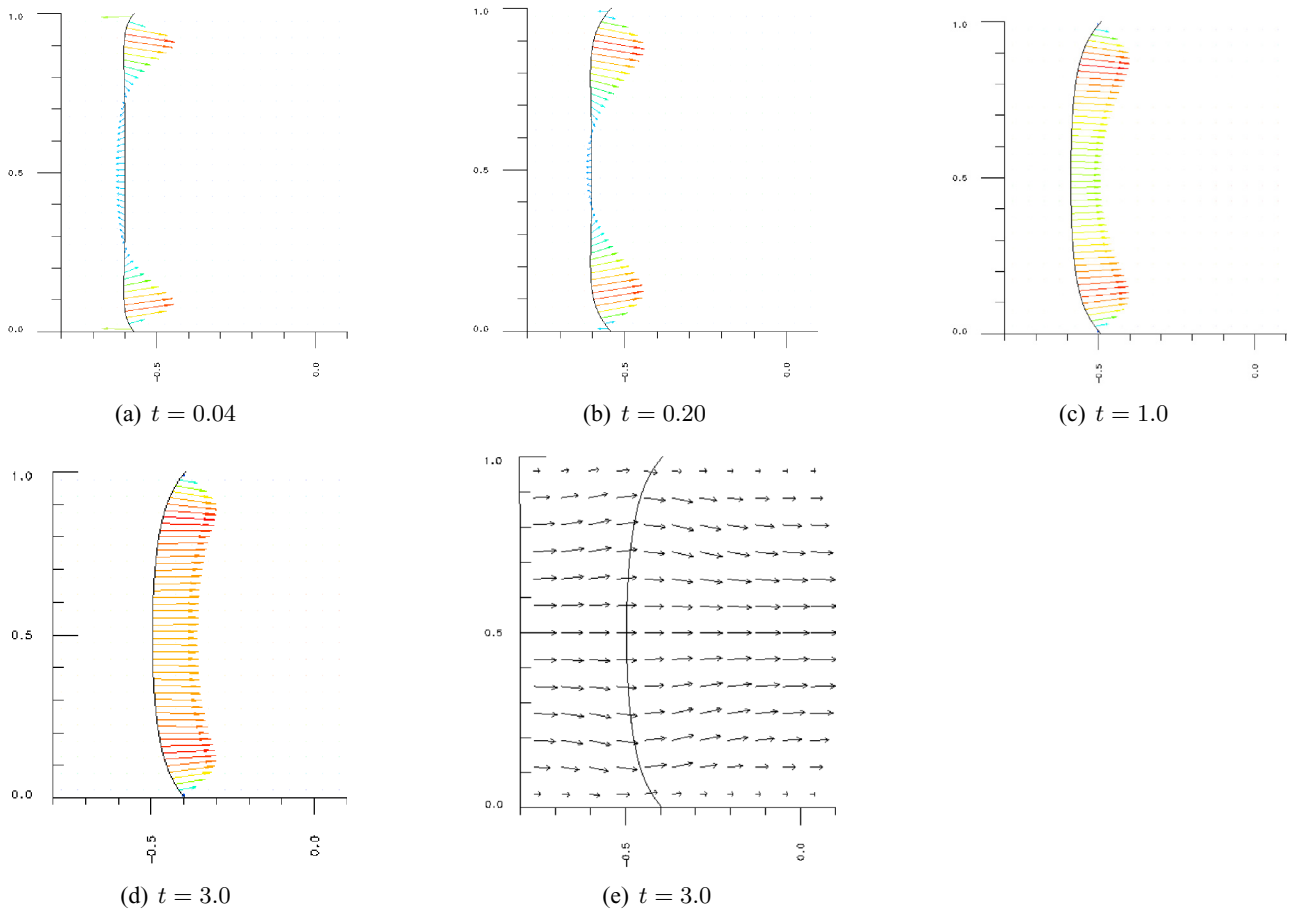

(a) $t = 0.04$ (b) $t = 0.20$ (c) $t = 1.0$

(d) $t = 3.0$ (e) $t = 3.0$

Figure 5: The location of the interface (the 0.5–level set of ϕ) at $t = 0.04, 0.2, 1.0, 3.0$. The arrows show the velocities. The angles at the upper and the lower channel walls are $\alpha = 45°$. The viscosity ratio $\frac{\mu_1}{\mu_2} = 1$.

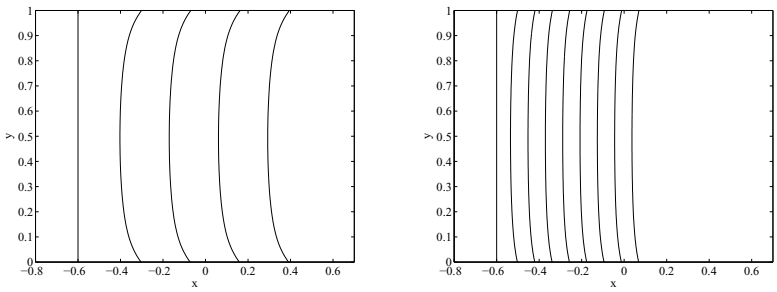

(a) $\alpha_s = 45°$ (b) $\alpha_{s_1} = 75°$

Figure 6: The location of the interface (the 0.5–level set of ϕ) at $t = 0, 5, 10, 15$, and 20 for two different static contact angles. The viscosity ratio $\frac{\mu_1}{\mu_2} = 1$.

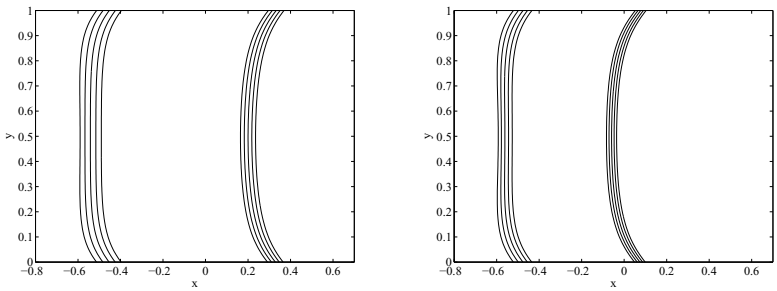

(a) $\frac{\mu_1}{\mu_2} = 4$ (b) $\frac{\mu_1}{\mu_2} = 8$

Figure 7: The location of the interface (the 0.5–level set of ϕ) at $t = 1, 2, 3, 4, 5, 36, 37, 38, 39, 40$. The angles at the upper and the lower channel walls are $\alpha_{s_1} = \alpha_{s_2} = 45°$. The fluid to the left is more viscous than the fluid to the right.

agreement with available theory and we observed better convergence compared to the calculations done in [9]. However, comparison with experiments and a better understanding of how the diffusion parameter and the regularization parameter should be chosen in order to resolve the curvature is needed before the model can be used for qualitative predictions.

ACKNOWLEDGEMENTS

The authors acknowledge Gustav Amberg, Minh Do–Quang, Anna–Karin Tornberg and Emanuel Rubensson for helpful discussions on fluid dynamics, Femlego and numerics. This project has partially been financed by Swedish Foundation for Strategic Research (SSF), Center for Industrial and applied mathematics at KTH (CIAM) and Linne Flow center at KTH.

REFERENCES

[1] P. G. de Gennes (1985). Wetting: statics and dynamics.*Rev. Mod. Phys.* **57**, 827–863.
[2] M. Renardy, Y. Renardy, J. Li (2001). Numerical simulation of moving contact line problems using a volume–of–fluid method. *J. Comput. Phys.* **171**, 243–263.
[3] T. Qian, Z.-P. Wang, P. Sheng (2006). Molecular hydrodynamics of the moving contact line in two–phase immiscible flows. *Comm. Comput. Phys.* **1**, 1–52.
[4] D. Jacqmin (2000). Contact-line dynamics of a diffuse fluid interface. *J. Fluid Mech.* **402**, 57–88.
[5] W. Villanueva, G. Amberg (2006). Some generic capillary-driven flows. *Int. J. Multiphase Flow* **32**, 1072–1086.
[6] E. Olsson, G. Kreiss (2005). A conservative level set method for two phase flow. *J. Comput. Phys.* **210**, 225–246.
[7] E. Olsson, G. Kreiss, S. Zahedi (2007). A conservative level set method for two phase flow II. *J. Comput. Phys.* **225**, 785–807.
[8] G. Kreiss (2007). *Modeling of contact line dynamics for two–phase flow*. ICIAM2007 proceedings.
[9] S. Zahedi, K. Gustavsson, G. Kreiss (2008). *A new model for contact line dynamics*. TRITA–NA, Royal Institute of Technology, Sweden, ISSN 0348–2952.
[10] E. Bänsch (1998). *Numerical methods for the instationary Navier–Stokes equations with a free capillary surface*. Habiliation thesis, University of Freiburg, Germany.
[11] S. Gross, A. Reusken (2007). Finite element discretization error analysis of a surface tension force in two–phase incompressible flows. *SIAM J. Numer. Anal.* **45**, 1679–1700.
[12] J. Sethian (1999). *Level Set Methods and Fast Marching Methods*. Cambridge University Press.
[13] S. Osher, R. Fedkiw (2003). Level Set Methods and Dynamic Implicit Surfaces. Springer–Verlag.
[14] A. Harten (1977). The artificial compression method for computation of shocks and contact discontinuities. I. Single conservation laws. *Comm. Pure Appl. Math.* **30** 611–638.
[15] J.–L. Guermond, L. Quartapelle (1997). Calculation of incompressible viscous flows by an unconditionally stable projection FEM. *J. Comput. Phys.* **132**, 12–33.
[16] G. Amberg, R. Tönhardt, C. Winkler (1999). Finite element simulations using symbolic computing. *Math. Comput. Simulat.* **49**, 257–274.
[17] R. G. Cox (1986). The dynamics of the spreading of liquids on a solid surface. Part1. Viscous flow. *J. Fluid Mech.* **168**, 169–194.

